CCS Chemistry

RESEARCH ARTICLE

Received: Mar. 21, 2024 | Accepted: Apr. 22, 2024 | Published: May 21, 2024

π-Fused Diazocines with Controllable Photoswitching Properties as Molecular Tweezers

Wei Yuan[1], Mengjiao Wu[2], Cheng Qian[1], Jingjing Guo[1], Yinglong Wu[1], Ting He[1], Haipeng Wei[3], Xiaokai Chen[1], Dongdong Wang[1], Jiawei Liu[1], Yue Zhao[1], Shihuai Wang[1], Jie Yang[1], Zhongzheng Zhang[1], Yulan Chen[2]* & Yanli Zhao[1]*

[1]*School of Chemistry, Chemical Engineering and Biotechnology, Nanyang Technological University, Singapore 637371,* [2]*State Key Laboratory of Supramolecular Structure and Materials, Jilin University, Changchun 130012,* [3]*Department of Chemistry, National University of Singapore, Singapore 117543*

**Corresponding authors: zhaoyanli@ntu.edu.sg; yulan.chen@jlu.edu.cn*

Cite this: *CCS Chem.* **2024**, 6, 2175–2185
DOI: 10.31635/ccschem.024.202404227

Diazocines, a type of photoswitch molecules, are distinguished by their unique conformation and photochromic properties. Molecular engineering of diazocines, especially the π-extended ones, remains challenging due to limited synthetic methods. Here, we developed three π-fused diazocines (BAZO-1, BAZO-2, and BAZO-3) via Bischler–Napieralski cyclization. Their isomerizations (*Z* ⇆ *E*) were switchable under visible light sources (427 and 630 nm). The size of their π-extension exerted a significant influence on the isomerization process, whereby the biggest fourfold ring-closure diazocine (BAZO-3) showed the fastest conversion rate (*Z* → *E*). Notably, the half-life ($t_{1/2}$) of the *E* isomer of BAZO-3 was 14.6 times higher than that of the twofold ring-closure BAZO-1. Thus, BAZO-3 acted as a molecular tweezer based on double *N*-embedded pyrene units, allowing it to bind to pyrene through supramolecular interactions. This work may pave the way for designing novel photoswitches with long half-lives and light-controlled properties.

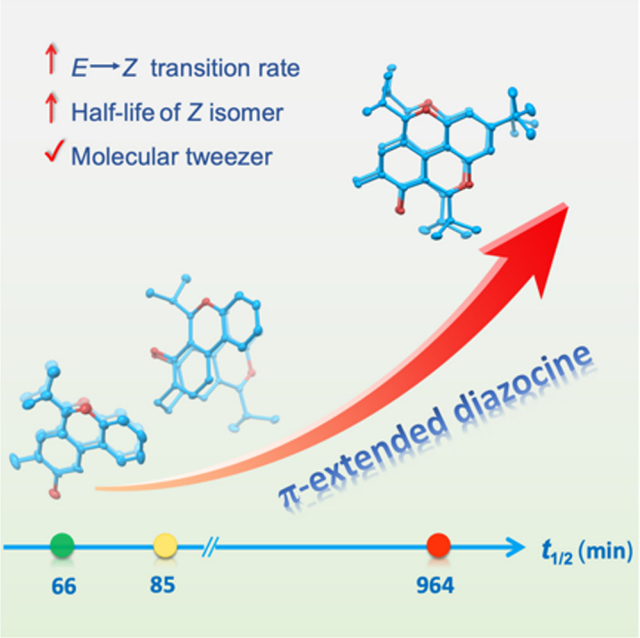

Keywords: diazocine, π-fused structure, photochromism, photoisomerization, molecular tweezer

Introduction

Photochromic molecules have gained immense attention for their wide applications in stimuli-responsive materials, molecule machines, and photoswitchable drug release.[1-8] Generally, they experience a reversible transformation between two isomers having different absorption spectra induced by photoirradiation. Photoswitching efficiency and sensitivity are two critical factors for their practical applications. So far, many studies

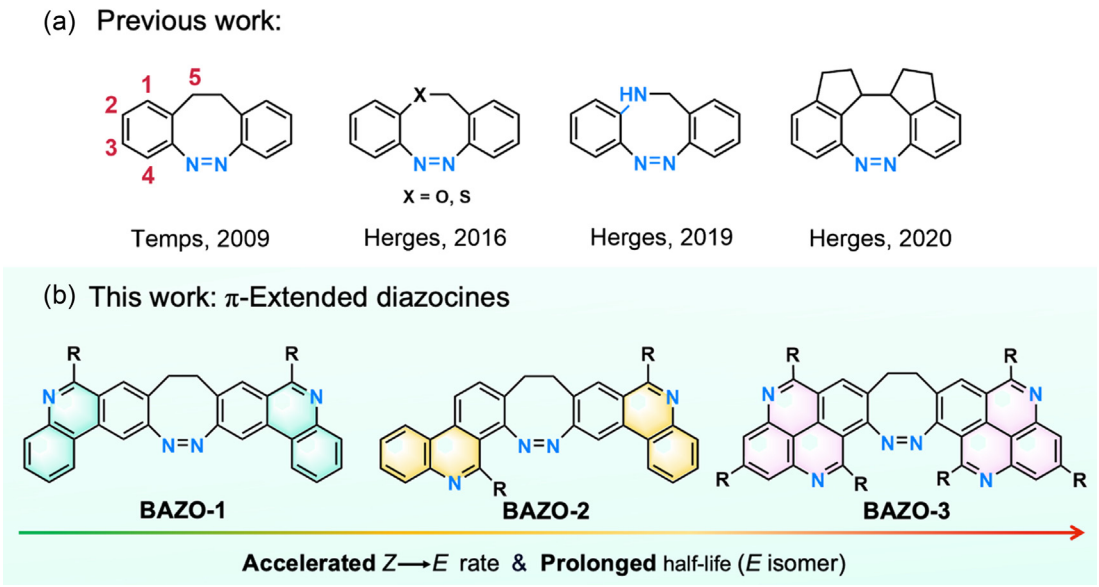

Scheme 1 | *Molecular engineering of diazocines (a) at the 1,5-positions and (b) at the 2,4-positions with π-extension for the generation of* ***BAZOs****.*

have been focused on the exploration of new photoswitching chromophores with high switching efficiency and sensitive responsiveness to low irradiated energy. One of the most widely explored chromophores is azobenzene and its derivatives.[9–12] However, the photoisomerization rate of most azobenzenes is relatively slow, owing to overlapping absorption bands of the two isomers between 400–500 nm.[13–15]

Complementary to azobenzenes, diazocines, which can be regarded as bridged azobenzenes, emerge as a new kind of molecular photoswitches. As displayed in Scheme 1a, diazocines contain an eight-membered ring via an ethylene bridge at the ortho position of the N=N bond.[16] Notably, the *Z* isomer is a thermodynamically favorable configuration due to the presence of ring strain, which has considerable advantages in the field of photopharmacology.[17] Meanwhile, the *Z* ⇆ *E* transition of diazocines is known to show a larger separation (100 nm) in absorption spectra through two suitable wavelengths, contributing to a faster photoisomerization rate, compared with azobenzenes. For azobenzene derivatives, the general principles between structure modification and photochemical properties such as the photoconversion yield, thermal half-life of *Z*-isomer, and photoresponse wavelength, have been defined.[18–21] However, these disciplines based on diazocines have not yet been investigated. The possible reason is that the structural diversity of diazocines is limited.[22,23] Notably, Herges group[24–26] and others[27] conducted research studies on the development of diazocines, mainly focusing on the incorporation of heteroatoms into the 1,5-positions (Scheme 1a). Herein, we focused on the development of π-fused diazocines. Generally, the bigger π-extended structures possessed enhanced absorption coefficient and redshifted absorption wavelength. The enlargement of the π-conjugated structure could increase molecular stability. Therefore, we expected that the π-extension of the diazocine core would offer great opportunities to tune their photochromic properties (such as photoresponse wavelength, photoisomerization rate, and half-life of metastable conformation) and enrich their functions. Thus, molecular engineering of π-extended diazocines was a highly desirable exploration.

In this context, we were interested in derivatives with larger π-fused rings at the 2,4 positions, since we envisaged that such new derivatization might offer more possibilities to tune the photophysical properties, configurations, and intermolecular interactions. To synthesize the π-extended diazocine; one standard approach is a reductive azo condensation of the π-extended precursor with two nitro groups. However, such a bigger structure often exhibits lower ring-closure reactivity owing to large steric hindrance. Therefore, we chose an alternative strategy. First, we obtained the dibromo derivatives of diazocine. Subsequently, we carried out a cyclization reaction to yield the π-extended diazocines. Given the versatility of the Bischler–Napieralski reaction to synthesize *N*-containing polycyclic aromatic hydrocarbons,[28–32] we developed a straightforward approach to design and synthesize three π-fused diazocines (**BAZO-1**, **BAZO-2**, and **BAZO-3**, Scheme 1b). This method effectively bypassed the challenges associated with the standard approach and allowed for the successful synthesis of π-extended diazocines. The three diazocines exhibited fast photoisomerization (*Z* ⇆ *E*) rates both in dilute solution and solid states. Due to the larger π-extended

DOI: 10.31635/ccschem.024.202404227
Citation: *CCS Chem.* **2024**, 6, 2175–2185
Link to VoR: https://doi.org/10.31635/ccschem.024.202404227

planar structure, **BAZO-3** showed an accelerated photoisomerization rate upon irradiation with blue light. Notably, the required wavelength of photoswitch for **BAZO-3** was redshifted compared with that of the parent diazocine ($\lambda_{Z\rightarrow E}$: 385 nm). In addition, the half-life of the *E* isomer of **BAZO-3** was 14.6 times longer than that of **BAZO-1**. This study unveiled a unique phenomenon that the biggest π-fused diazocines possessed not only the fastest photoinduced transition (from *Z* to *E*) but also the longest half-life of the *E* isomer, highlighting the influence of the π-extension on the photoreactive properties of photochromic molecules. Benefiting from a symmetrical π-extended saddle-shaped structure, **BAZO-3** could act as a host, effectively binding to pyrene to form a supramolecular complex in a 1:1 molar ratio. This observation signified the applications of **BAZO-3** as a photoswitchable molecular tweezer.

Experimental Methods

Unless otherwise noted, all chemicals were purchased from Merck or TCI both in Singapore, and used without further purification. Dichloromethane (CH_2Cl_2) was distilled over CaH_2. Tetrahydrofuran (THF) was distilled over sodium and benzophenone. All reactions were performed under an argon atmosphere and monitored by TLC with silica gel 60 and fluorescent indicator F254 coated plate (60 F254; Merck, Singapore). Column chromatography was carried out on silica gel (200–300 mesh; Merck, Singapore). Detailed synthetic procedures are shown in Supporting Information Scheme S1 and Scheme 2a,b, and nuclear magnetic resonance (NMR) spectra of all the compounds are shown in the Supporting Information.

Synthetic procedure for compound 2

Compound **1** was synthesized and characterized according to the literature.[17] A mixture of 2-aminophenylboronic acid (500 mg, 3.65 mmol), compound **1** (640 mg, 1.75 mmol), K_2CO_3 (966 mg, 7.0 mmol), and $Pd(PPh_3)_4$ (161 mg, 0.14 mmol) in 1,4-dioxane/H_2O (30 mL/5 mL), placed in a two-neck flask, degassed, then refluxed overnight under argon. After quenching the reaction, 1,4-dioxane was evaporated under reduced pressure, then the remaining solution was extracted with CH_2Cl_2 (3 × 50 mL). The combined organic layer was dried over sodium sulfate. The crude product was purified by column chromatography on silica gel (hexane/ethyl acetate = 5:1, v/v) to give compound **2** as a light yellow solid (409 mg, 1.05 mmol, yield: 60%). ^{1}H NMR (400 MHz, $CDCl_3$, ppm, δ): 7.14–7.07 (m, 3H), 7.01–6.99 (dd, *J* = 7.6 Hz, 1H), 6.93–6.92 (d, *J* = 2.4 Hz, 1H), 6.79–6.75 (t, *J* = 8.0 Hz, 1H), 6.71–6.69 (d, *J* = 8.0 Hz, 1H), 3.56 (br, 2H), 3.08–3.05 (m, 1H), 2.86–2.84 (m, 1H). ^{13}C NMR (100 MHz, $CDCl_3$, ppm, δ): 155.9, 143.44, 138.2, 130.3, 130.2, 128.8, 127.8, 127.2, 126.2, 118.9, 118.7, 115.7, 31.4. Electrospray ionization mass spectrometry (ESI-MS) (*m*/*z*): calcd for $C_{26}H_{22}N_4$ 390.1844; found 391.1835 $[M + H]^+$.

Synthetic procedure for compound 3

To a dry THF solution (20 mL) of compound **2** (400 mg, 1.02 mmol) and triethylamine (1 mL) was added dropwise a dry THF solution (10 mL) of isobutyryl chloride (326 mg, 3.06 mmol) at 0 °C. After stirring at room temperature for 10 min, the solution was poured into water (80 mL) and extracted with CH_2Cl_2 (3 × 80 mL). The combined organic layer was dried over anhydrous sodium sulfate and evaporated to dryness. The residue was purified by

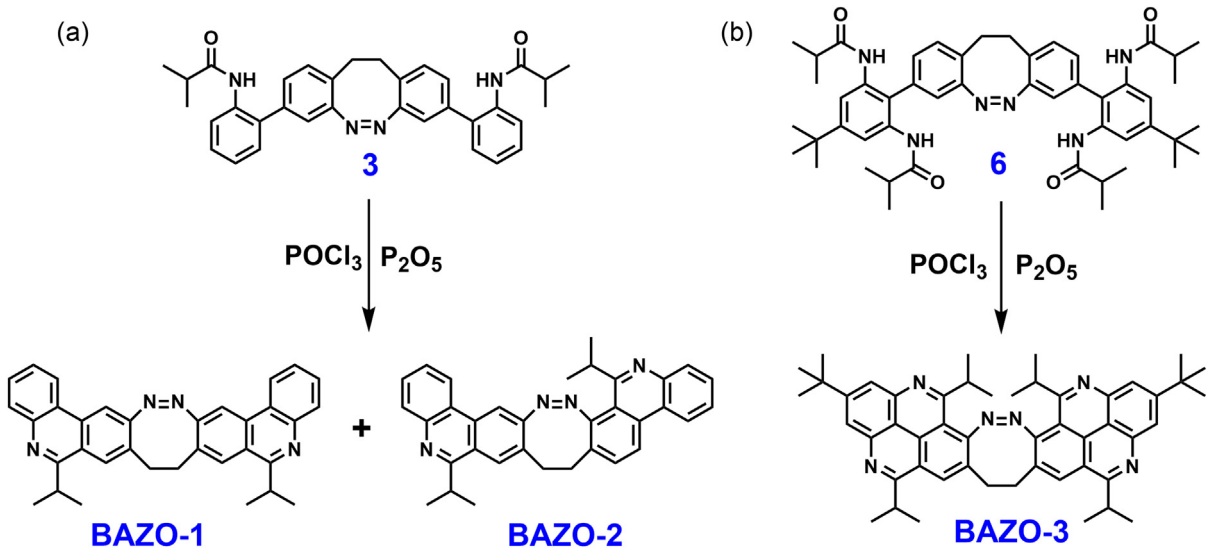

Scheme 2 | *Synthetic route of **BAZOs**.*

DOI: 10.31635/ccschem.024.202404227
Citation: *CCS Chem.* **2024**, 6, 2175–2185
Link to VoR: https://doi.org/10.31635/ccschem.024.202404227

chromatography on a silica gel column eluting with hexane/ethyl acetate (5:1, v/v) to afford compound **3** as a white solid (347.7 mg, 0.65 mmol, yield: 64%). ^{1}H NMR (400 MHz, CD_2Cl_2, ppm, δ): 7.85–7.83 (d, *J* = 8.0 Hz, 1H), 7.33–7.08 (m, 6H), 6.86 (s, 1H), 3.06–3.03 (m, 1H), 2.89–2.85 (m, 1H), 2.14–2.10 (m, 1H), 0.89–0.87 (d, *J* = 8.0 Hz, 3H), 0.81–0.79 (d, *J* = 8.0 Hz, 3H). ^{13}C NMR (100 MHz, CD_2Cl_2, ppm, δ): 174.8, 156.0, 137.5, 134.8, 133.0, 130.2, 130.0, 128.3, 127.82, 127.7, 125.0, 123.6, 119.1, 35.8, 31.2, 29.7, 19.1, 19.0. ESI-MS (*m/z*): calcd for $C_{34}H_{34}N_4O_2$ 530.2682; found 531.2737 $[M + H]^+$.

Synthetic procedure for compound 4

To a dry THF solution (30 mL) containing 2-bromo-5-(tert-butyl)benzene-1,3-diamine (1.21 g, 5 mmol) and triethylamine (1 mL) were added dropwise to a dry THF solution (10 mL) containing isobutyryl chloride (1.63 g, 15.2 mmol) at 0 °C. After stirring at room temperature for 10 min, the solution was poured into water (80 mL) and extracted with CH_2Cl_2 (3 × 100 mL). The combined organic layer was dried over anhydrous sodium sulfate and evaporated to dryness. The residue was purified by chromatography on a silica gel column (hexane/ethyl acetate = 3:1, v/v) to afford compound **4** as a white solid (1.15 g, 3 mmol, yield: 60%). ^{1}H NMR (400 MHz, $CDCl_3$, ppm, δ): 8.17 (s, 2H), 7.56 (s, 2H), 2.62–2.59 (m, 2H), 1.33–1.30 (m, 21H). ^{13}C NMR (100 MHz, $CDCl_3$, ppm, δ): 175.1, 152.3, 135.3, 115.7, 37.0, 35.1, 31.1, 19.6. ESI-MS (*m/z*): calcd for $C_{18}H_{27}N_2O_2Br$ 382.1256; found 383.1359 $[M + H]^+$.

Synthetic procedure for compound 5

A mixture of compound **1** (1.0 g, 2.73 mmol), bis(pinacolato)diboron (1.90 g, 7.30 mmol), KOAc (0.600 g, 6.60 mmol), and $Pd(dppf)Cl_2$ (0.100 g, 0.140 mmol) in 1,4-dioxane (50 mL) was placed in a two-neck flask, and heated under reflux for 24 h under Ar atmosphere. After cooling to room temperature, the mixture was poured into deionized water and extracted with CH_2Cl_2. The organic phase was dried with anhydrous sodium sulfate, filtered, and evaporated to dryness. The residue was purified by flash chromatographically (hexane/CH_2Cl_2 = 1:1) to provide compound **5** as a yellow solid (0.90 g, 1.97 mmol, 72%). ^{1}H NMR (400 MHz, $CDCl_3$, ppm, δ): 7.44–7.42 (d, *J* = 8.0 Hz, 1H), 7.29 (s, 1H), 6.99–6.97 (d, *J* = 8.0 Hz, 1H), 3.03–2.99 (m, 1H), 2.80–2.76 (m, 1H), 1.31–1.30 (d, 12H). ^{13}C NMR (100 MHz, $CDCl_3$, ppm, δ): 155.0, 133.5, 131.0, 129.0, 125.5, 84.0, 32.0, 25.0, 24.8. ESI-MS (*m/z*): calcd for $C_{26}H_{34}B_2N_2O_4$ 460.2705; found 461.2765 $[M + H]^+$.

Synthetic procedure for compound 6

A mixture of compound **4** (725.8 mg, 1.9 mmol), compound **5** (420 mg, 0.91 mmol), K_2CO_3 (496.8 mg, 3.6 mmol), and $Pd(dppf)Cl_2$ (33.3 mg, 0.05 mmol) in 1,2-dimethoxyethane/H_2O (30 mL/5 mL) was placed in a two-neck flask, degassed, then refluxed overnight under argon atmosphere. After quenching the reaction, the generated 1,2-dimethoxyethane was evaporated under reduced pressure, and then the remaining solution was extracted with CH_2Cl_2 (3 × 80 mL). The combined organic layer was dried over anhydrous sodium sulfate. The crude product was purified by column chromatography on silica gel (hexane/ethyl acetate = 5:2, v/v) to give compound **6** as a light yellow solid (309 mg, 0.38 mmol, yield: 42%). ^{1}H NMR (400 MHz, THF-d_8, ppm, δ): 8.35 (s, 2H), 7.91–7.85 (d, 4H), 7.27 (s, 2H), 7.04–7.02 (d, *J* = 8.0 Hz, 2H), 6.96–6.94 (d, *J* = 8.0 Hz, 2H), 6.76 (s, 2H), 2.98–2.96 (m, 2H), 2.83–2.81 (m, 2H), 2.40–2.36 (m, 2H), 2.08–2.06 (m, 2H), 1.29 (s, 18H), 0.70–0.68 (m, 12H), 0.50–0.48 (m, 12H). ^{13}C NMR (100 MHz, THF-d_8, ppm, δ): 174.4, 173.9, 156.3, 156.2, 150.4, 135.7, 133.9, 129.5, 129.3, 127.3, 124.6, 120.4, 119.3, 118.5, 35.5, 34.5, 34.4, 31.2, 30.6, 18.9, 18.8, 18.4. ESI-MS (*m/z*): calcd for $C_{50}H_{64}N_6O_4$ 812.4989; found 813.5266 $[M + H]^+$.

Synthetic procedure for compounds BAZO-1 and BAZO-2

A solution of compound **3** (100 mg, 0.19 mmol), P_2O_5 (127.7 mg, 0.9 mmol), and $POCl_3$ (10 mL) was placed in a two-neck flask, heated to reflux, and stirred under argon for 18 h. The mixture was cooled to room temperature, then added dropwise into NaOH solution (6 M), and stirred for 30 min. The aqueous solution was adjusted to pH = 9–10 and extracted with CH_2Cl_2 (3 × 30 mL). The combined organic layers were dried over anhydrous sodium sulfate and evaporated to dryness. The product was purified by chromatography on silica gel column eluting with $CHCl_3$ to obtain **BAZO-1** and **BAZO-2**, respectively. The residue was recrystallized in CH_2Cl_2/hexane to afford light yellow solid: **BAZO-1** (22.6 mg, 0.046 mmol, yield: 24%); **BAZO-2** (15.0 mg, 0.031 mmol, yield: 16%).

BAZO-1: ^{1}H NMR (400 MHz, CD_2Cl_2, ppm, δ): 8.37–8.35 (d, *J* = 8.0 Hz, 1H), 8.07 (s, 1H), 7.96–7.92 (m, 2H), 7.63–7.59 (t, *J* = 8.0 Hz, 1H), 7.54–7.51 (t, *J* = 8.0 Hz, 1H), 3.81 (m, 1H), 3.31–3.25 (m, 2H), 1.42–1.40 (d, *J* = 8.0 Hz, 3H), 1.31–1.29 (d, *J* = 8.0 Hz, 3H). ^{13}C NMR (100 MHz, CD_2Cl_2, ppm, δ): 165.4, 157.7, 144.1, 132.5, 130.0, 129.4, 129.1, 127.5, 126.6, 123.9, 123.3, 122.3, 112.4, 32.3, 31.7, 30.1, 22.2, 21.9. ESI-MS (*m/z*): calcd for $C_{34}H_{30}N_4$ 494.2470; found 495.2491 $[M + H]^+$.

BAZO-2: ^{1}H NMR (400 MHz, CD_2Cl_2, ppm, δ): 8.43–8.41 (d, *J* = 8.0 Hz, 1H), 8.37–8.35 (d, *J* = 8.0 Hz, 1H), 8.25–8.23 (d, *J* = 8.0 Hz, 1H), 7.96–7.89 (m, 3H), 7.87 (s, 1H), 7.64–7.58 (m, 3H), 7.52–7.48 (t, *J* = 8.0 Hz, 2H), 3.97 (m, 1H), 3.79 (m, 1H), 3.56 (m, 1H), 3.23 (m, 1H), 3.08 (m, 2H), 1.56–1.52 (m, 6H), 1.40–1.38 (d, *J* = 8.0 Hz, 3H), 1.32–1.30 (d, *J* = 8.0 Hz, 3H). ^{13}C NMR (100 MHz, CD_2Cl_2, ppm, δ): 164.9, 164.5, 153.4, 133.3, 131.6, 131.0, 129.2, 128.7, 127.2, 126.5, 126.2, 123.3, 122.8, 122.4, 121.8, 121.5, 117.0, 111.0, 34.6, 34.2,

DOI: 10.31635/ccschem.024.202404227
Citation: *CCS Chem.* **2024**, 6, 2175–2185
Link to VoR: https://doi.org/10.31635/ccschem.024.202404227

31.9, 31.2, 31.1, 30.5, 30.0, 29.7, 23.3, 22.7, 22.5, 21.9, 21.3, 13.9. ESI-MS (*m/z*): calcd for $C_{34}H_{30}N_4$ 494.2470; found 495.2470 $[M + H]^+$.

Synthetic procedure for compounds BAZO-3

A solution of compound **6** (100 mg, 0.13 mmol), P_2O_5 (113.5 mg, 0.4 mmol), and $POCl_3$ (10 mL) placed in a two-neck flask, heated to reflux and stirred under argon for 18 h. The mixture was cooled to room temperature, then added dropwise into NaOH solution (6 M), and stirred for 30 min. The aqueous solution was adjusted to pH = 9–10 and extracted with $CHCl_3$ (3 × 50 mL). The combined organic layers were dried over anhydrous sodium sulfate and evaporated to dryness. The crude product was purified by chromatography on a silica gel column (hexane/CH_2Cl_2 = 4:3, v/v) to give compound **BAZO-3** as a light yellow solid (11.5 mg, 0.016 mmol, yield: 12%). ^{1}H NMR (400 MHz, $CDCl_3$, ppm, δ): 8.22 (d, *J* = 1.6 Hz, 2H), 8.20 (d, *J* = 1.6 Hz, 2H), 8.16 (s, 2H), 3.92–3.83 (m, 4H), 3.68–3.66 (m, 2H), 3.47–3.45 (m, 2H), 1.68–1.66 (m, 6H), 1.52–1.50 (m, 12H), 1.49 (s, 18H), 1.32–1.26 (m, 6H). ^{13}C NMR (100 MHz, CD_2Cl_2, ppm, δ): 165.4, 164.0, 153.6, 152.3, 141.6, 141.1, 128.7, 127.6, 126.4, 123.3, 122.7, 122.4, 114.1, 109.4, 35.9, 35.7, 33.7, 32.0, 31.8, 31.7, 29.8, 24.5, 22.1, 21.7, 20.7. ESI-MS (*m/z*): calcd for $C_{50}H_{56}N_6$ 740.4566; found 741.4775 $[M + H]^+$.

Theoretical calculation method

All density functional theory (DFT) calculations were carried out using Gaussian 09. Geometries of intermediates and transition states were optimized using the B3LYP-D3(BJ) function with the 6-31g(d, p) basis set using Grimme's DFT-D3 dispersion correction.[33] Vibrational frequency calculations were performed for all the stationary points to confirm if each optimized structure was a local minimum or a transition state. The B3LYP-D3 (BJ) function was used in single-point energy calculations with the 6-311++g(d,p) basis set using Grimme's DFT-D3 dispersion correction in toluene solvent with the solvation model density (SMD) continuum solvation model.[34] The three-dimensional (3D) images of the computed structures were prepared using CYLView.[35]

Results and Discussion

As shown in Supporting Information Scheme S1, starting from (Z)-3,8-dibromo-11,12-dihydrodibenzo[c,g]-[1,2] diazocine (compound **1**), the diamino precursor **2** was obtained by the Suzuki-Miyaura reaction. Subsequently, compound **3** was synthesized through the amidation reaction in the presence of isobutyryl chloride. Interestingly, since compound **3** had two regioselective sites to undergo the Bischler–Napieralski cyclization reaction, **BAZO-1** and **BAZO-2** were obtained simultaneously. To our delight, **BAZO-3**, possessing the biggest π-extension was obtained successfully by a fourfold Bischler–Napieralski cyclization reaction of compound **6**. These molecules were characterized by NMR (^{1}H and ^{13}C), high-resolution mass spectroscopy, and single-crystal X-ray diffraction (XRD) analysis (Supporting Information Tables S1–S3).

The single crystals of **BAZO-1**, **BAZO-2**, and **BAZO-3** were generated successfully by slow evaporation of mixed solvents (see Supporting Information). Single crystallographic analysis revealed that they possessed unique saddle-shaped structures, and all adopted the *Z* configuration in their natural condition, similar to previous diazocines, but completely different from normal azobenzenes. For **BAZO-1**, part of the ethylene bridge and N=N bond was almost coplanar, and the carbon-nitrogen-nitrogen (CNN) and carbon-carbon-carbon (CCC) chain bond angles of the eight-membered ring were 120.7° and 116.5°, almost identical to the angle of the sp^2 bond (Figure 1a). The dihedral angle formed by the two azaphenanthrene surfaces in **BAZO-1** was 71.39° (Supporting Information Figure S1). For **BAZO-2**, the CNN and CCC angles were 118.2° and 112.9°, resulting in slight distortion for the central CNNC moiety (Figure 1b). Its dihedral angle was 80.64° (Supporting Information Figure S2). Driven by multiple intermolecular interactions such as C–H···C–H and C–H···π (distance from 2.25 to 2.81 Å), **BAZO-1** formed ordered columnar stacking. Different from the parallel stacking model in **BAZO-1** under π–π stacking interaction, the neighboring **BAZO-2** molecules revealed no π–π stacking. For **BAZO-3**, the CNN and CCC angles were 117.7° and 113.5° (Figure 1c), and there was no π–π stacking interaction with surrounding molecules (Supporting Information Figure S3). Notably, the dihedral angle between the double *N*-embedded pyrene unit is 51.3°, much smaller than **BAZO-1** and **BAZO-2** (Figure 1d). Subtle changes in the size of π-extension for

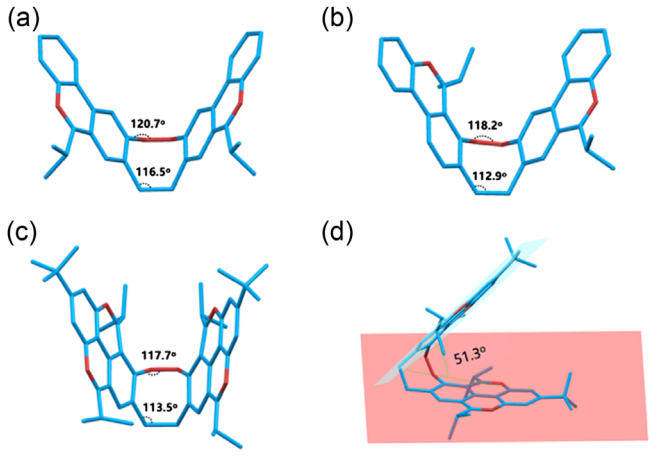

Figure 1 | *Crystal structures of (a)* ***BAZO-1****, (b)* ***BAZO-2****, and (c)* ***BAZO-3****. (d) Dihedral angle between the double N-embedded pyrene units in* ***BAZO-3****.*

DOI: 10.31635/ccschem.024.202404227
Citation: *CCS Chem.* **2024**, 6, 2175–2185
Link to VoR: https://doi.org/10.31635/ccschem.024.202404227

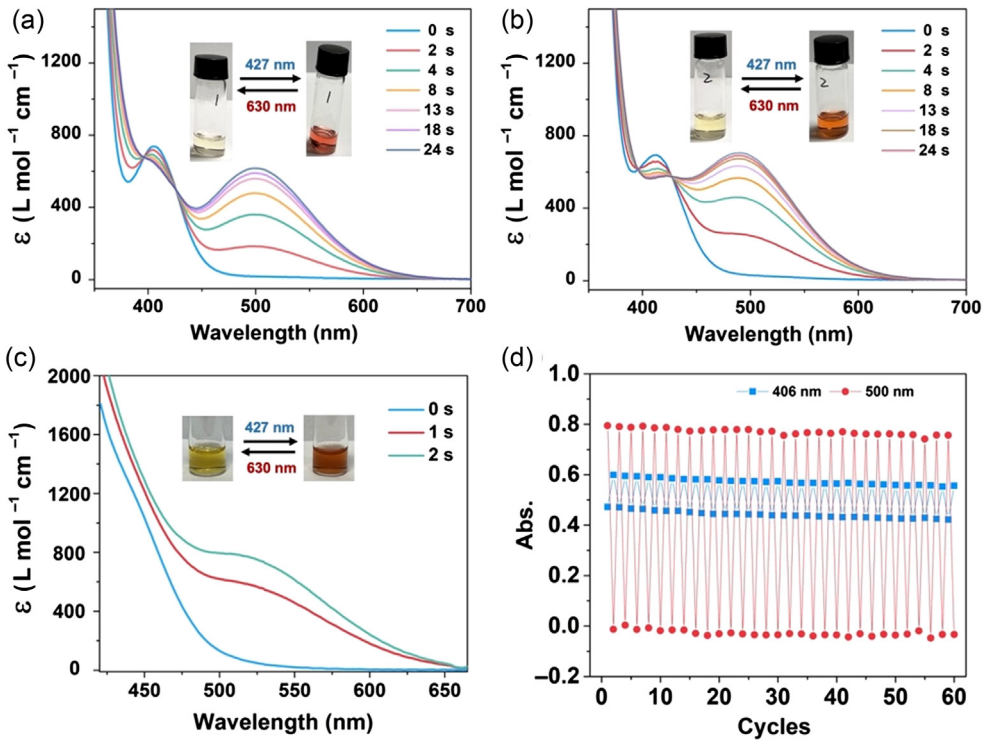

Figure 2 | *UV–vis spectra of (a)* ***BAZO-1****, (b)* ***BAZO-2****, and (c)* ***BAZO-3*** *in THF solution upon irradiation with 427 nm. (d) Measured absorbance of* ***BAZO-1*** *in THF solution at* λ_1 *= 406 nm (blue) and* λ_2 *= 500 nm (red) upon alternating irradiation using 405 and 630 nm light sources. All the concentrations are 1 × 10*$^{-3}$ *M.*

diazocine brought profound differences in the molecular conformation. Generally, there is an inverse relationship between interplanar angles and torsion angles, meaning that molecules with larger interplanar angles tend to exhibit a smaller sum of all torsion angles.[36,37] Thus, we hypothesized that this phenomenon arose from the bigger substituents in compound **6**, leading to a larger sum of all torsion angles compared with compound **3**. As a result, the interplanar angle of **BAZO-3** was smaller than those in **BAZO-1** and **BAZO-2**.

The photoisomerization of these diazocines was investigated in THF solution. Compared with parent diazocine, the three π-extended diazocines possessed a larger π-conjugated framework, expected to realize photoisomerization under the low-energy visible light region. As shown in Supporting Information Figures S4 and S5, when we used 405 nm light to irradiate the THF solution of **BAZO-1**, the absorption intensity at 406 nm (ascribed to n–π* transition) was slightly decreased with the prolongation of exposure time.[38] Meanwhile, a new peak at 500 nm appeared and was gradually enhanced, accompanied by a significant color change of the solution from pale yellow to brown. **BAZO-2** showed a similar change in absorption spectrum (Supporting Information Figures S6 and S7). Then we used 427 nm light to irradiate the **BAZO-1** and **BAZO-2** solutions; the two systems reached the photostationary state (PSS) in 20 and 24 s, respectively (Figure 2a,b). The maximum absorption wavelengths for *E* isomers of **BAZO-1** and **BAZO-2** were 500 and 490 nm respectively, due to the discrepancy of their π-conjugation directions. These definite spectral changes validated the transition from *Z* to *E* form. The photoreaction constants of **BAZO-1** and **BAZO-2** were determined to be 0.214 and 0.215 s^{-1} respectively, which were two orders of magnitude higher than conventional azobenzenes (Supporting Information Figure S8).[39] Since **BAZO-3** had a larger π-extension, it exhibited an enhanced absorption coefficient at 427 nm. As expected, the PSS time of **BAZO-3** was only 2 s in the same condition (Figure 2c), suggesting the photoisomerization rate as follows: **BAZO-3** > **BAZO-1** ≈ **BAZO-2**.

Their photoisomerization was further confirmed by the ^{1}H NMR spectroscopy (Supporting Information Figures S9–S11). The detailed photochemical properties are summarized in Supporting Information Table S4. Their absorption bands for *E* isomers were broad and extended up to 650 nm, allowing for a red light source (λ = 630 nm) usage to induce the *E* → *Z* transition. Up to 60 cycles of switch experiments did not show fatigue, demonstrating their excellent photostability (Figure 2d and Supporting Information Figures S12–S16). In addition to light-induced transformation (*E* → *Z*), heating their PSS solution (1 × 10^{-3} M) enabled this process (Supporting Information Figures S17–S19). Apart from solution studies, we investigated their photoswitchable properties in the solid phase. On a filter paper with polyethylene glycol

DOI: 10.31635/ccschem.024.202404227
Citation: *CCS Chem.* **2024**, 6, 2175–2185
Link to VoR: https://doi.org/10.31635/ccschem.024.202404227

(Mn = 5000) as a passivation layer, when three colorless letters were written with a dilute **BAZO-1** solution (1 mg/mL), three light pink letters, NTU,- appeared upon irradiation with 427 nm light, demonstrating the photoswitching in the solid state (Supporting Information Figure S20a). After irradiation with 630 nm light or heat treatment, these letters disappeared immediately. This process could be repeated without fatigue. Therefore, **BAZO-1** could be used to construct a rewritten paper. Meanwhile, **BAZO-2** had a similar behavior (Supporting Information Figure S20b). These above experiments demonstrated that these novel diazocines exhibited excellent photochromic properties both in solution and the solid state.

We then investigated the thermal stability of the substable *E* isomer. Thermal relaxation kinetics of these three diazocines from *E* to *Z* isomers were monitored by UV–vis spectroscopy in THF solution (1×10^{-3} M). It was found that all of them followed first-order kinetics, and the half-lives ($t_{1/2}$) of their *E* isomers were determined as 66, 85, and 964 min respectively (Figure 3a,b and Supporting Information Figure S21). The thermal isomerization half-life of a photochromic molecule was a critical factor that determined its practical usability. Azobenzene has been systematically investigated in this aspect. Through structural engineering of azobenzene, it was possible to effectively tune the half-life range from a few seconds to several years. For diazocine, due to the limited research in this area, there was still a lack of a set of guidelines and rules for designing new diazocines with a long half-life. In this study, it is worth noting that the fourfold ring-closure structure (**BAZO-3**) considerably enhanced the thermal stability of the *E* isomer, exhibiting 14.6 times and 11.3 larger than that of the twofold ring-closure ones (**BAZO-1** and **BAZO-2**), respectively. The π-extension-induced increase of half-life ($t_{1/2}$) has not been previously documented in previous photochromic molecules. This distinct phenomenon would stand as a new rulebook for the designing of novel photoswitches. Based on these findings, we proposed that the incorporation of double *N*-embedded pyrene structures greatly

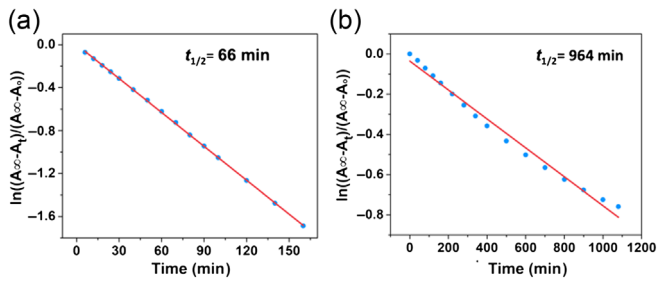

Figure 3 | *Half-lives ($t_{1/2}$) of the subthermal* E *isomer of (a)* ***BAZO-1*** *and (b)* ***BAZO-3*** *measured in THF solution at 25 °C (1×10^{-3} M).*

increased the intermolecular steric repulsion effect, which further hampered the rotation of the diazocine core, and consequently stabilized the *E* isomer.[20] In addition, since the isopropyl groups were located farther from the N=N bond, their impact was minor relative to the larger π-extension. Therefore, owing to the bigger π-extension, the half-life of the *E* isomer of **BAZO-3** was longer than those for **BAZO-1** and **BAZO-2**.

To reveal the transition process of *Z* and *E* isomers, we performed DFT (the B3LYP/6-311++g(d,p)-D3BJ-SMD (THF)/B3LYP/6-31g(d,p)-D3BJ method) to evaluate the configurational energy landscape of these diazocines in different forms. Similar to the previously reported diazocines, their *Z* isomers were more stable than their *E* isomers. Taking **BAZO-3** as an example, the *E* isomer had two possible conformations, namely chair (C1) and twist (T1), which were in equilibrium (Figure 4). The twist conformation (T1) was 3.5 kcal/mol more stable than the chair conformation (C1), and the activation barrier for the twist (T1) → chair (C1) interconversion was 15.7 kcal/mol via TS1. A similar transformation process was involved for **BAZO-1** and **BAZO-2** (Supporting Information Figures S22 and S23). Remarkably, from *Z* isomer to *E* isomer (twist conformation), the activation barrier (2.0 kcal/mol) of **BAZO-3** was much smaller than that of **BAZO-1** (8.7 kcal/mol) and **BAZO-2** (7.5 kcal/mol), which was in good agreement with the experimental data. This explained the photoisomerization rate as follows: **BAZO-3** > **BAZO-1** ≈ **BAZO-2**.

Next, we used the variable temperature NMR technology to investigate the detailed transition process from the *Z* to *E* isomer of **BAZO-1**. After irradiation, the peaks of the aromatic moiety (7.5–9.0 ppm), bridged ethylene (3.4–3.2 ppm), and isopropyl group (1.3–1.4 ppm) were markedly changed, which gave evidence for the generation of *E* isomer (Figure 5). When the temperature dropped from 298 to 243 K, the proton signal of bridged-C_2 became complicated from two singlet peaks into multiple peaks (3.1–3.4 ppm), which provided strong evidence for the presence of several conformations in equilibrium (such as twist and chair forms). The experimental results were consistent with the theoretical calculations. For **BAZO-2**, significant changes were also presented in variable temperature NMR spectra upon irradiation. When the temperature decreased to 253 K, multiple peaks emerged from 3.6 to 4.1 ppm (Supporting Information Figure S24). The methyl signal of the isopropyl group became complicated with expected multiplicities, which also directly proved the dynamic transition between the chair and twist conformations. In contrast to the bridged methylene and isopropyl position, aromatic signals of **BAZO-1** and **BAZO-2** were observed to remain unchanged upon decreasing the temperature after the irradiation. One possible explanation was attributed to a fast interconversion between chair ⇆ twist conformation to result in a time-averaged NMR signal. Another reason

DOI: 10.31635/ccschem.024.202404227
Citation: *CCS Chem.* **2024**, 6, 2175–2185
Link to VoR: https://doi.org/10.31635/ccschem.024.202404227

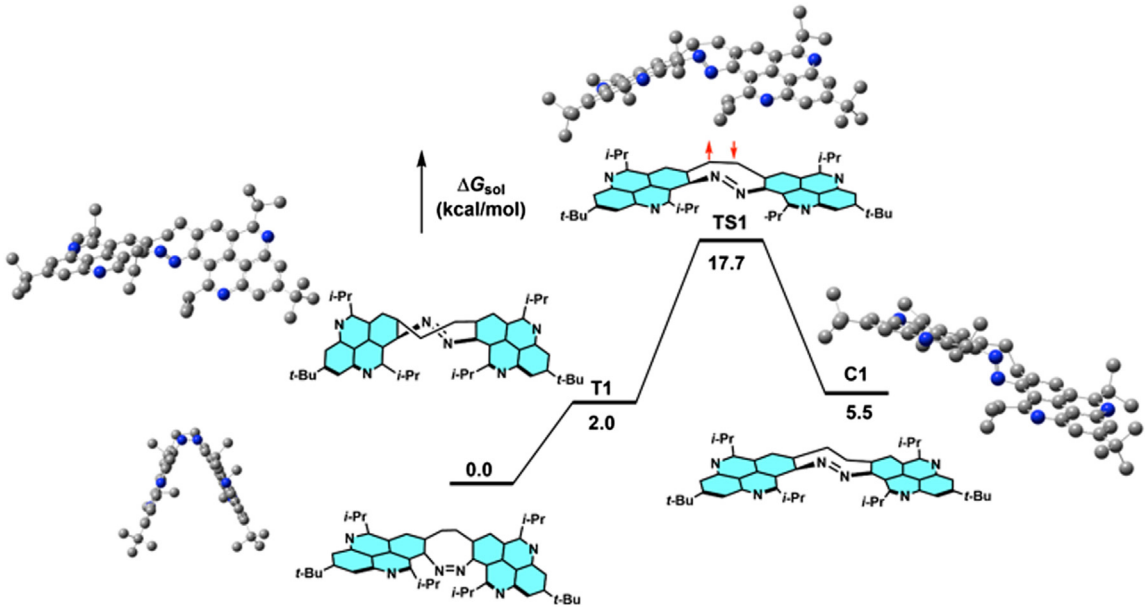

Figure 4 | *Calculated total energy of **BAZO-3** with different conformations. Each conformation was optimized in gas. Energies of* E *isomers (twist, TS1, and chair conformations) relative to the corresponding* Z *isomers in kcal/mol.*

could be that one of the two conformations dominated, making the other below the detection limit in equilibrium. As noted above, the *E* isomers of **BAZO-1** and **BAZO-2** included two conformations (chair and twist), which were in equilibrium with rapid conformation exchange at room temperature. Due to the temperature decrease of **BAZO-3**, clear peak changes were observed from 3.4 to 3.7 ppm (Supporting Information Figure S25), suggesting the existence of conformation exchange between twist and chair forms.

The development of photoswitchable molecular hosts is of great significance but extremely challenging.[40–43] Inspired by the symmetric saddle-shaped structure, we speculated that the π-electron-deficient and deep cavity of **BAZO-3** might allow it to recognize electron-rich aromatic compounds through supramolecular interactions. Given the presence of double *N*-embedded pyrene units, we initially selected pyrene as an electron-rich guest to pair with **BAZO-3**, thereby constructing a supramolecular host–guest system. A Job plot obtained from fluorescent measurements indicated a 1:1 binding ratio in the THF solution (Supporting Information Figures S26 and S27a). The fluorescence intensity of pyrene was gradually quenched with the addition of **BAZO-3** (Figure 6a). The binding constant (Ka) was determined as $2.25 \pm 0.04 \times 10^4$ M^{-1} for the **BAZO-3**@Pyrene complex

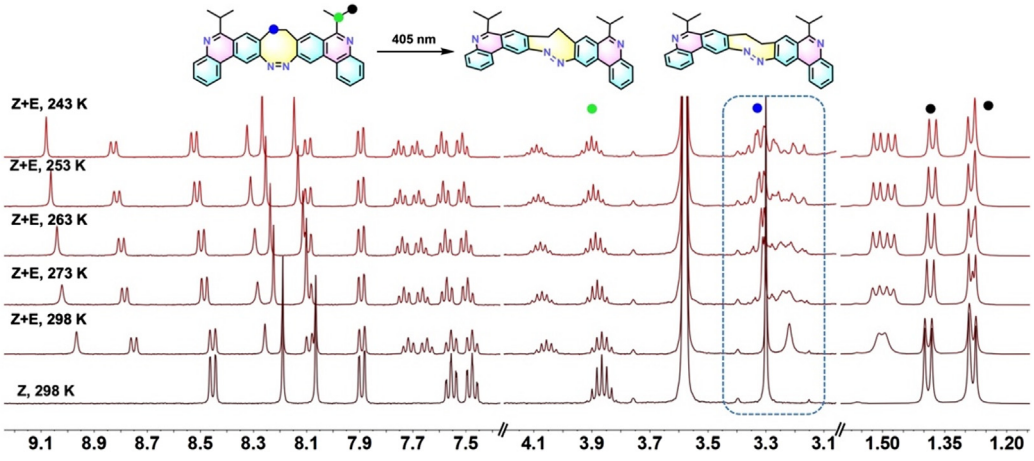

Figure 5 | *^{1}H NMR spectra of **BAZO-1** in THF-d_8 at different temperatures after irradiation with a 405 nm light source. The different color spheres are indicative of the NMR signals for the corresponding positions.*

DOI: 10.31635/ccschem.024.202404227
Citation: *CCS Chem.* **2024**, 6, 2175–2185
Link to VoR: https://doi.org/10.31635/ccschem.024.202404227

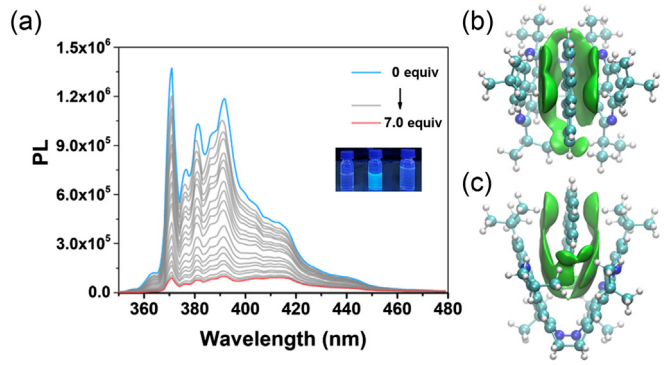

Figure 6 | *(a) Fluorometric titration spectra of pyrene (2×10^{-5} M) with **BAZO-3** (up to 1.4×10^{-4} M). Inset from left to right: fluorescence image of **BAZO-3**, Pyrene, and **BAZO-3**@Pyrene under 365 nm UV illumination. (b) Top and (c) side views of IGM analysis for **BAZO-3**@Pyrene complex.*

through fluorometric titration spectra, confirming the robust host–guest interactions.[44] To acquire a deep comprehension of the interaction between the **BAZO-3** and pyrene, a joint investigation of independent gradient model (IGM) analysis was performed (Figure 6b,c), which revealed that the pyrene was embedded in the center of the cavity of **BAZO-3** with the help of π–π and multiple CH–π interactions. Additionally, the highest occupied molecular orbital (HOMO) and lowest unoccupied molecular orbital (LUMO) energy for the complex was obtained; it showed that the HOMO was dominated by the pyrene, and the charge of the LUMO orbital was located on the **BAZO-3** (Supporting Information Figure S27b,c). The observed charge separation of HOMO and LUMO levels indicated a donor–acceptor interaction between the *N*-embedded pyrene and parent pyrene unit, which was also supported by the shortened fluorescence lifetime of pyrene from 18.7 to 17.2 ns (Supporting Information Figure S28). Consequently, the adaptive cavity and electron-withdrawing property might make **BAZO-3** become a host to encapsulate sizeable organic guests. Considering its distinctive structure and photoswitchable properties, **BAZO-3** is expected to be a versatile core for constructing photoswitchable molecular tweezers in the future.

Conclusion

We have successfully constructed three π-fused diazocines via the Bischler–Napieralski cyclization as a key step (Characterization spectra are shown in Supporting Information Figures S29–S52). Their *Z* isomers were proven to be more thermodynamically stable than their *E* counterparts, established through obtained single-crystal structures and spectroscopic analyses. Benefiting from a larger π-conjugated structure than the parent diazocine, isomerizations ($Z \leftrightarrows E$) could be activated under visible light (427 and 630 nm). More importantly, the enlarged π-extension of the diazocines not only accelerated the photoisomerization rate but prolonged the half-life of the *E* isomer (from 66 to 964 min). Meanwhile, the $E \rightarrow Z$ conversion efficiency was as high as 99% upon red light (630 nm) irradiation. Photoisomerization experiments showed no fatigue over 60 cycles. The multiple conformation interconversion of their *E* isomers was confirmed via variable temperature NMR analysis and DFT calculations. Interestingly, **BAZO-3** possessed a saddle-shaped structure, conducive to the formation of supramolecular complex **BAZO-3**@Pyrene, aided by donor–acceptor interactions. These findings open up new avenues for designing stable photoswitches and photocontrolled releases.

Supporting Information

Supporting Information is available and includes the supplemental experimental details, Scheme S1, Figures S1–S52, and Tables S1–S4.

Conflict of Interest

There is no conflict of interest to report.

Funding Information

This research was supported financially by the Singapore Agency for Science, Technology, and Research (A*STAR) under its Manufacturing, Trade and Connectivity Individual Research Grant (IRG; grant no. M22K2c0077) and National Natural Science Foundation of China (NSFC; grant no. 21975178).

References

1. Szymanski, W.; Beierle, J. M.; Kistemaker, H. A.; Velema, W. A.; Feringa, B. L. Reversible Photocontrol of Biological Systems by the Incorporation of Molecular Photoswitches. *Chem. Rev.* **2013**, *113*, 6114–6178.
2. Qian, H.; Pramanik, S.; Aprahamian, I. Photochromic Hydrazone Switches with Extremely Long Thermal Half-Lives. *J. Am. Chem. Soc.* **2017**, *139*, 9140–9143.
3. Qian, H.; Wang, Y.-Y.; Guo, D.-S.; Aprahamian, I. Controlling the Isomerization Rate of an Azo-BF_2 Switch Using Aggregation. *J. Am. Chem. Soc.* **2017**, *139*, 1037–1040.
4. Kay, E. R.; Leigh, D. A.; Zerbetto, F. Synthetic Molecular Motors and Mechanical Machines. *Angew. Chem. Int. Ed.* **2007**, *46*, 72–191.
5. Xu, T.-Y.; Tong, F.; Xu, H.; Wang, M.-Q.; Tian, H.; Qu, D.-H. Engineering Photomechanical Molecular Crystals to Achieve Extraordinary Expansion Based on Solid-State [2+2] Photocycloaddition. *J. Am. Chem. Soc.* **2022**, *144*, 6278–6290.

DOI: 10.31635/ccschem.024.202404227
Citation: *CCS Chem.* **2024**, 6, 2175–2185
Link to VoR: https://doi.org/10.31635/ccschem.024.202404227

6. Morstein, J.; Awale, M.; Reymond, J.-L.; Trauner, D. Mapping the Azolog Space Enables the Optical Control of New Biological Targets. *ACS Cent. Sci.* **2019**, *5*, 607–618.
7. Yu, F.; Liu, W.; Li, B.; Tian, D.; Zuo, J; Zhang, Q. Photostimulus-Responsive Large-Area Two-Dimensional Covalent Organic Framework Films. *Angew. Chem. Int. Ed.* **2019**, *58*, 16101–16104.
8. She, P.; Qin, Y.; Wang, X.; Zhang, Q. Recent Progress in External-Stimulus-Responsive 2D Covalent Organic Frameworks. *Adv. Mater.* **2022**, *34*, 2101175.
9. Hartley, G. S. The Cis-Form of Azobenzene. *Nature* **1937**, *140*, 281.
10. Merino, E.; Ribagorda, M. Control over Molecular Motion Using the Cis–Trans Photoisomerization of the Azo Group. *Beilstein J. Org. Chem.* **2012**, *8*, 1071–1090.
11. Bléger, D.; Hecht, S. Visible-Light-Activated Molecular Switches. *Angew. Chem. Int. Ed.* **2015**, *54*, 11338–11349.
12. Liu, G.; Sheng, J.; Teo, W. L.; Yang, G.; Wu, H.; Li, Y.; Zhao, Y. Control on Dimensions and Supramolecular Chirality of Self-Assemblies Through Light and Metal Ions. *J. Am. Chem. Soc.* **2018**, *140*, 16275–16283.
13. Merino, E. Synthesis of Azobenzenes: The Coloured Pieces of Molecular Materials. *Chem. Soc. Rev.* **2011**, *40*, 3835–3853.
14. Zhou, H.; Xue, C.; Weis, P.; Suzuki, Y.; Huang, S.; Koynov, K.; Auernhammer, G. K.; Berger, R.; Butt, H.-J.; Wu, S. Photoswitching of Glass Transition Temperatures of Azobenzene-Containing Polymers Induces Reversible Solid-to-Liquid Transitions. *Nat. Chem.* **2017**, *9*, 145–151.
15. Bandara, H. D.; Burdette, S. C. Photoisomerization in Different Classes of Azobenzene. *Chem. Soc. Rev.* **2012**, *41*, 1809–1825.
16. Siewertsen, R.; Neumann, H.; Buchheim-Stehn, B.; Herges, R.; Nather, C.; Renth, F.; Temps, F. Highly Efficient Reversible Z–E Photoisomerization of a Bridged Azobenzene with Visible Light through Resolved S_1 ($n\pi^*$) Absorption Bands. *J. Am. Chem. Soc.* **2009**, *131*, 15594–15595.
17. Cabré, G.; Garrido-Charles, A.; González-Lafont, À.; Moormann, W.; Langbehn, D.; Egea, D.; Lluch, J. M.; Herges, R.; Alibés, R.; Busqué, F. Synthetic Photoswitchable Neurotransmitters Based on Bridged Azobenzenes. *Org. Lett.* **2019**, *21*, 3780–3784.
18. Calbo, J.; Weston, C. E.; White, A. J.; Rzepa, H. S.; Contreras-García, J.; Fuchter, M. J. Tuning Azoheteroarene Photoswitch Performance Through Heteroaryl Design. *J. Am. Chem. Soc.* **2017**, *139*, 1261–1274.
19. Lameijer, L. N.; Budzak, S.; Simeth, N. A.; Hansen, M. J.; Feringa, B. L.; Jacquemin, D.; Szymanski, W. General Principles for the Design of Visible-Light-Responsive Photoswitches: Tetra-Ortho-Chloro-Azobenzenes. *Angew. Chem. Int. Ed.* **2020**, *59*, 21663–21670.
20. Schweighauser, L.; Strauss, M. A.; Bellotto, S.; Wegner, H. A. Attraction or Repulsion? London Dispersion Forces Control Azobenzene Switches. *Angew. Chem. Int. Ed.* **2015**, *54*, 13436–13439.
21. Dang, T.; Dong, D.; Zhang, J.; He, Y.; Zhang, Z. Y.; Li, T. Thiazolylazopyrazoles as Nonsymmetric Bis-Heteroaryl Azo Switches: High-Yield Visible-Light Photoisomerization and Increased Z-Isomer Stability by o-Carbonylation. *Angew. Chem. Int. Ed.* **2023**, *62*, e202301992.
22. Joshi, D. K.; Mitchell, M. J.; Bruce, D.; Lough, A. J.; Yan, H. Synthesis of Cyclic Azobenzene Analogues. *Tetrahedron* **2012**, *68*, 8670–8676.
23. Thorwirth, R.; Bernhardt, F.; Stolle, A.; Ondruschka, B.; Asghari, J. Switchable Selectivity During Oxidation of Anilines in a Ball Mill. *Chem. Eur. J.* **2010**, *16*, 13236–13242.
24. Hammerich, M.; Schütt, C.; Stähler, C.; Lentes, P.; Röhricht, F.; Höppner, R.; Herges, R. Heterodiazocines: Synthesis and Photochromic Properties, Trans to Cis Switching within the Bio-Optical Window. *J. Am. Chem. Soc.* **2016**, *138*, 13111–13114.
25. Lentes, P.; Stadler, E.; Röhricht, F.; Brahms, A.; Gröbner, J.; Sönnichsen, F. D.; Gescheidt, G.; Herges, R. Nitrogen Bridged Diazocines: Photochromes Switching within the Near-Infrared Region with High Quantum Yields in Organic Solvents and in Water. *J. Am. Chem. Soc.* **2019**, *141*, 13592–13600.
26. Moormann, W.; Tellkamp, T.; Stadler, E.; Röhricht, F.; Näther, C.; Puttreddy, R.; Rissanen, K.; Gescheidt, G.; Herges, R. Efficient Conversion of Light to Chemical Energy: Directional, Chiral Photoswitches with Very High Quantum Yields. *Angew. Chem. Int. Ed.* **2020**, *59*, 15081–15086.
27. Samanta, S.; Qin, C.; Lough, A. J.; Woolley, G. A. Bidirectional Photocontrol of Peptide Conformation with a Bridged Azobenzene Derivative. *Angew. Chem. Int. Ed.* **2012**, *51*, 6452–6455.
28. Min, L.; Yang, W.; Weng, Y.; Zheng, W.; Wang, X.; Hu, Y. A Method for Bischler–Napieralski-Type Synthesis of 3,4-Dihydroisoquinolines. *Org. Lett.* **2019**, *21*, 2574–2577.
29. Han, Y.; Hu, Z.; Liu, M.; Li, M.; Wang, T.; Chen, Y. Synthesis, Characterization, and Properties of Diazapyrenes via Bischler–Napieralski Reaction. *J. Org. Chem.* **2019**, *84*, 3953–3959.
30. Yuan, W.; Cheng, J.; Li, X.; Wu, M.; Han, Y.; Yan, C.; Zou, G.; Müllen, K.; Chen, Y. 5,6,12,13-Tetraazaperopyrenes as Unique Photonic and Mechanochromic Fluorophores. *Angew. Chem. Int. Ed.* **2020**, *59*, 9940–9945.
31. Yuan, W.; Ren, X. K.; Li, M.; Guo, H.; Han, Y.; Wu, M.; Wang, Q.; Li, M.; Chen, Y. From S,N-Heteroacene to Large Discotic Polycyclic Aromatic Hydrocarbons (PAHs): Liquid Crystal Versus Plastic Crystalline Materials with Tunable Mechanochromic Fluorescence. *Angew. Chem. Int. Ed.* **2018**, *57*, 6161–6165.
32. Kou, Y.; Li, G.; Han, Y.; Li, M.; Wang, T.; Qu, Z.; Chen, Y. Angularly Fused Diaza-Dinaphthopyrenes: Regio-Selective Synthesis, Crystal Structures and Isomer-Dependent Mechanochromic Fluorescent Properties. *Chem. Sci.* **2023**, *14*, 668–674.
33. Grimme, S.; Antony, J.; Ehrlich, S.; Krieg, H. A Consistent and Accurate ab Initio Parametrization of Density Functional Dispersion Correction (DFT-D) for the 94 Elements H-Pu. *J. Chem. Phys.* **2010**, *132*, 154104.
34. Marenich, A. V.; Cramer, C. J.; Truhlar, D. G. Universal Solvation Model Based on Solute Electron Density and on a Continuum Model of the Solvent Defined by the Bulk Dielectric Constant and Atomic Surface Tensions. *J. Phys. Chem. B* **2009**, *113*, 6378–6396.

DOI: 10.31635/ccschem.024.202404227
Citation: *CCS Chem.* **2024**, 6, 2175–2185
Link to VoR: https://doi.org/10.31635/ccschem.024.202404227

35. Legault, C. *CYLview, 1.0 b*; Université de Sherbrooke: Sherbrooke, Canada, **2009**.
36. Reger, D.; Haines, P.; Amsharov, K.; Schmidt, J.; Ullrich, T.; Bönisch, S.; Hampel, F.; Görling, A.; Nelson, J.; Jelfs, K.; Guldi, D.; Jux, N. A Family of Superhelicenes: Easily Tunable, Chiral Nanographenes by Merging Helicity with Planar π Systems. *Angew. Chem. Int. Ed.* **2021**, *60*, 18073–18081.
37. Duke, R.; Bhat, V.; Smith, A.; Goodlett, S.; Tretiak, S.; Risko, C. Factors Impacting Dihedral Angle Rotation and Classification in π-Conjugated Systems. *Macromolecules* **2023**, *56*, 5259–5267.
38. Wang, Y.; Li, M.; Yan, C.; Ma, N.; Chen, Y. Diazocine as a Versatile Building Block Enables Excellent Photoswitching and Chromic Properties in Self-Assembled Organogels. *CCS Chem.* **2022**, *4*, 704–712.
39. Zhu, Q.; Wang, S.; Chen, P. Diazocine Derivatives: A Family of Azobenzenes for Photochromism with Highly Enhanced Turn-On Fluorescence. *Org. Lett.* **2019**, *21*, 4025–4029.
40. Liu, Y. M.; Xia, D.; Li, B. W.; Zhang, Q. Y.; Sakurai, T.; Tan, Y. Z.; Seki, S.; Xie, S. Y.; Zheng, L. S. Functional Sulfur-Doped Buckybowls and Their Concave–Convex Supramolecular Assembly with Fullerenes. *Angew. Chem. Int. Ed.* **2016**, *55*, 13047–13051.
41. Tellkamp, T.; Shen, J.; Okamoto, Y.; Herges, R. Diazocines on Molecular Platforms. *Eur. J. Org. Chem.* **2014**, *2014*, 5456–5461.
42. Hardouin-Lerouge, M.; Hudhomme, P.; Salle, M. Molecular Clips and Tweezers Hosting Neutral Guests. *Chem Soc. Rev.* **2011**, *40*, 30–43.
43. Wu, H.; Chen, Y.; Zhang, L.; Anamimoghadam, O.; Shen, D.; Liu, Z.; Cai, K.; Pezzato, C.; Stern, C. L.; Liu, Y. A Dynamic Tetracationic Macrocycle Exhibiting Photoswitchable Molecular Encapsulation. *J. Am. Chem. Soc.* **2018**, *141*, 1280–1289.
44. Thordarson, P. Determining Association Constants from Titration Experiments in Supramolecular Chemistry. *Chem. Soc. Rev.* **2011**, *40*, 1305–1323.

DOI: 10.31635/ccschem.024.202404227
Citation: *CCS Chem.* **2024**, 6, 2175–2185
Link to VoR: https://doi.org/10.31635/ccschem.024.202404227